Article

A vanadium(III) complex with blue and NIR-II spin-flip luminescence in solution

Matthias Dorn, Jens Kalmbach, Pit Boden, Ayla Päpcke, Sandra Gomez, Christoph Förster, Felix Kuczelinis, Luca M. Carrella, Laura Büldt, Nicolas Bings, Eva Rentschler, Stefan Lochbrunner, Leticia Gonzalez, Markus Gerhards, Michael Seitz, and Katja Heinze

Just Accepted

A vanadium(III) complex with blue and NIR-II spin-flip luminescence in solution

Matthias Dorn[1], Jens Kalmbach[2], Pit Boden[3], Ayla Päpcke[4], Sandra Gómez[5], Christoph Förster[1], Felix Kuczelinis[1], Luca M. Carrella[1], Laura Büldt[2], Nicolas Bings[1], Eva Rentschler[1], Stefan Lochbrunner[4], Leticia González[5], Markus Gerhards*[3], Michael Seitz*[2] and Katja Heinze*[1]

[1] Department of Chemistry, Johannes Gutenberg University of Mainz, Duesbergweg 10-14, 55128 Mainz, Germany.

[2] Institute of Inorganic Chemistry, University of Tübingen, Auf der Morgenstelle 18, 72076 Tübingen, Germany.

[3] Department of Chemistry and Research Center Optimas, Technical University Kaiserslautern, Erwin-Schrödinger-Straße, 67663 Kaiserslautern, Germany.

[4] Institute for Physics and Department of Life, Light and Matter, University of Rostock, 18051 Rostock, Germany.

[5] Institute of Theoretical Chemistry, Faculty of Chemistry, University of Vienna, Währinger Straße 17, 1090 Vienna, Austria.

Key words: NIR emitter; Earth-abundant metals, vanadium; nitrogen ligands; quantum chemical calculations; photophysics; ligand field splitting

Abstract Luminescence from Earth-abundant metal ions in solution at room temperature is a very challenging objective due to the intrinsically weak ligand field splitting of first row transition metal ions, which leads to efficient non-radiative deactivation via metal-centered states. Only a handful of $3d^n$ metal complexes ($n \neq 10$) show sizeable luminescence at room temperature. Luminescence in the near-infrared spectral region is even more difficult to achieve as further non-radiative pathways come into play. No Earth-abundant first-row transition metal complexes display emission > 1000 nm at room temperature in solution up to now. Here we report the vanadium(III) complex *mer*-[V(ddpd)$_2$][PF$_6$]$_3$ yielding phosphorescence around 1100 nm in valeronitrile glass at 77 K as well as at room temperature in acetonitrile with 1.8×10^{-4} % quantum yield (ddpd = *N,N'*-dimethyl-*N,N'*-dipyridine-2-ylpyridine-2,6-diamine). In addition, *mer*-[V(ddpd)$_2$][PF$_6$]$_3$ shows very strong blue fluorescence with 2 % quantum yield in acetonitrile at room temperature. Our comprehensive study demonstrates that vanadium(III) complexes with d^2 electron configuration constitute a new class of blue and NIR-II luminophores, which complement the classical established complexes of expensive precious metals and rare-earth elements.

Introduction

Luminescent complexes of Earth-abundant metal ions started to emerge only in the last few years.[1-4] Typically, the abundant first row transition metal ions are prone to sub-picosecond non-radiative relaxation via low-energy metal-centered (MC) states, which precluded any useful emission until recently.[4-6] The majority of the very few reported room-temperature luminescent complexes possess rather long-lived charge transfer (CT) states thanks to a high energy or absence of the detrimental MC states. A d^6-chromium(0) complex with isocyanide ligands shows ^{3}MLCT (metal-to-ligand CT) emission at 630 nm (τ = 2.2 ns, Φ = 0.001 %).[7] d^6-Cobalt(III) complexes with tridentate strong field ligands display blue emission from ^{3}LMCT (ligand-to-metal) states (440/412 nm, τ = 5.1/3.2+8.7 ns, Φ = 0.7/0.4 %).[8] Fluorescence from ^{2}LMCT states is induced in d^5-iron(III) complexes using carbene ligands (655 nm, τ = 1.96 ns, Φ = 2.1 %).[9,10] Copper(I) complexes can exhibit quantum yields up tp 100 %, e.g. two-coordinate d^{10}-copper(I) complexes of cyclic (alkyl)(amino)carbene and amide ligands emit from ligand-to-ligand charge transfer (LLCT) states between 492 – 580 nm (τ = 280 – 2500 ns, Φ = 11 – 100 %).[11] Clearly, the visible spectral region started to be covered by 3d CT emitters, yet room-temperature near-infrared (NIR-I: 780 – 1000 nm; NIR-II: 1000 – 1700 nm) emission in solution has not yet been reported with CT complexes of Earth-abundant metal ions. On the other hand, strong NIR luminescence has been achieved exploiting the spin-flip emission of d^3-chromium(III) complexes using tridentate strong field ligands, leading to the so-called molecular rubies [Cr(L)$_2$]$^{3+}$ (L = e.g. ddpd, tpe; ddpd = N,N'-dimethyl-N,N'-dipyridine-2-ylpyridine-2,6-diamine; tpe = 1,1,1-tris(pyrid-2-yl)ethane; 782 – 724 nm, τ = 670 – 4500 µs, Φ = 5.2 – 30 %, CH$_3$CN).[12-17] However, emission above 900 nm or even above 1000 nm (NIR-II) at room-temperature remains elusive with 3d metal complexes in solution.

In principle, near-infrared (NIR) luminescence enables exciting applications in telecommunications, laser and LED/OLED or LEC technologies (OLED = organic light emitting diode, LEC = light-emitting electrochemical cell) as well as in bio-analysis and bio-imaging.[18-22] NIR-II luminescence can be particularly beneficial for in vivo imaging with respect to tissue penetration as well as reduced auto-fluorescence of the background and scattering losses.[18,19] Current materials are based on rare-earth elements, precious metals and organic dyes often in conjunction with precious metals.[23-28] The rare-earth ions typically display comparably sharp emission bands, yet split by electron-electron repulsion, spin-orbit coupling and the crystal field.[29] Organic emitters often show broad emission bands which typically merely tail into the NIR spectral region, hence, some emission still occurs in the visible spectral region.

A fundamental problem of low-energy emission derives from the energy-gap law especially for distorted excited states. The rate constant for non-radiative decay that reduces the luminescence quantum yield Φ increases with decreasing energy difference between the emitting and the ground state.[30,31] Nested, i.e. weakly distorted states (such as f-f and d-d spin-flip transitions) are hence better suited for NIR emission. Furthermore, high-energy oscillators, e.g. OH from water or CH from coordinating ligands, can increase non-radiative decay via energy transfer to suitable OH/CH vibrational overtones.[32,33] Lanthanide compounds, e.g. Nd, Sm, Dy or Yb, very often embedded in nanoparticles which lack detrimental CH oscillators, achieve NIR-II luminescence due to their favorable excited state levels originating from f-f transitions and the absence of high-energy oscillators.[18,19,29] The quantum yields for molecular NIR emissive lanthanide complexes are rather small, although deuterated cage and fluorinated porphyrin complexes of Yb^{3+} showing emission around 1000 nm recently achieved exceptionally high quantum yields.[34-36] However, rare-earth elements and precious metals are difficult and expensive to mine and purify, so that a huge interest arose in replacing these elements with Earth-abundant metals in luminescence applications.[1-4]

Analogous to the d^3 electron configuration of the abundant metal chromium(III),[2,12-17] an excited state ordering with low-energy spin-flip states (^{1}E$_g$/^{1}T$_{2g}$) emerges from a d^2 electron configuration in an octahedral ligand field (^{3}T$_{1g}$ ground state), provided that a strong ligand field is imposed to increase the energy gap between the interconfigurational triplet state (^{3}T$_{2g}$) and the intraconfigurational singlet states (^{1}E$_g$/^{1}T$_{2g}$ < ^{3}T$_{2g}$ at Δ_o > 17.3 B in the standard Tanabe-Sugano diagram; see Supporting Information, Figure S1; Δ_o and B are

the ligand field parameters). We hypothesized, that this situation can be realized by octahedral vanadium(III) complexes in a strong ligand field. The energy of potentially emissive singlet states of vanadium(III) has been determined by absorption spectroscopy on classical vanadium(III) compounds with O-donor ligands, such as V^{3+}:Al_2O_3, $[V(H_2O)_6]^{3+}$, $[V(urea)_6]^{3+}$ and $[V(ox)_3]^{3-}$,[37-41] and by 2p3d resonant inelastic X-ray scattering on $V(acac)_3$ as ~10000 cm^{-1} (~ 1000 nm) (urea = $OC(NH_2)_2$, ox = $[C_2O_4]^{2-}$, acac = $[CH_3(CO)CH(CO)CH_3]^-$).[42] This energy excellently matches the targeted window for luminescence applications in the NIR-II region. However, the known vanadium(III) compounds display after excitation and intersystem crossing (ISC) only very weak phosphorescence at low temperature, if phosphorescence is observed at all.[37-41] For example, the phosphorescence intensity of V^{3+}:Al_2O_3 is 3-4 orders of magnitude smaller than that of the R lines of ruby (Cr^{3+}:Al_2O_3) and the vanadium(III) spin-flip emission has been only detected in the solid state at low temperatures so far.[37,38] Instead, (delayed) fluorescence from vanadium centered $^3T_{2g}$ states occurs in compounds with ligand field strengths close to 17.3 B.[43,44] Consequently, back-ISC from ^1E_g/$^1T_{2g}$ to $^3T_{2g}$ states must be suppressed. This can in principle be achieved by further increasing the ligand field strength thus shifting the $^3T_{2g}$ states to higher energy relative to the singlet states. On the other hand, to promote ISC from the triplets to the singlet manifold besides large spin-orbit coupling, a high density of singlet states in the energy region of the $^3T_{2g}$ states is beneficial.[45] According to ligand field theory, an additional singlet term ($^1A_{1g}$) crosses the $^3T_{2g}$ term at very high ligand field strengths (Δ_o > 36.6 B in the standard Tanabe-Sugano diagram; Supporting Information, Figure S1). Consequently, an even larger ligand field splitting than Δ_o >> 17.3 B, namely $\Delta_o \approx 36.6$ B, could be advantageous to promote ISC to the singlet states via the high-energy $^1A_{1g}$ state in vanadium(III) complexes. In this study, such a large ligand field splitting will be targeted.

The strong-field ligand ddpd already enabled spectacular room temperature quantum yields above 10 % and μs-lifetimes in solution in the prototypical molecular ruby $[Cr(ddpd)_2]^{3+}$.[12] Ligand and solvent deuteration even boosted the quantum yield to 30 % and the lifetime to 2300 μs.[13] However, an analogous coordination chemistry of vanadium(III) and oligopyridine ligands is underdeveloped.[46,47] *cis-fac*-$[V(ddpd)_2][PF_6]_3$x3 CH_3CN is the first reported stable homoleptic polypyridine vanadium(III) complex.[46] Yet, the bond lengths in *cis-fac*-$[M(ddpd)_2]^{n+}$ isomers are typically longer than in *mer*-isomers due to the ligand deformation, which reduces the actual ligand field strength.[46]

Here we demonstrate, that the strong field ligand ddpd promotes ISC in a novel close-to-octahedral vanadium(III) complex *mer*-$[V(ddpd)_2][PF_6]_3$. Consequently, the complex shows NIR-II phosphorescence at low as well as at room temperature in solution. In addition, a strong blue fluorescence is observed. To deeper elucidate the key challenges for luminescent vanadium(III) complexes, we recorded fs-transient absorption spectra and ns-step-scan FTIR spectra for *mer*-$[V(ddpd)_2][PF_6]_3$. In order to judge the influence of multiphonon relaxation via CH overtones, we prepared and studied the deuterated analogue $[V([D_{17}]$-ddpd)$_2][PF_6]_3$. Static quantum chemical and non-adiabatic molecular dynamics simulations provide a comprehensive insight into the electronic excited state properties and ultrafast dynamics of *mer*-$[V(ddpd)_2]^{3+}$.

Results

Synthesis, X-ray structure and Characterization of $[V^{III}(ddpd)_2]^{3+}$

The dark green complex *mer*-$[V^{III}(ddpd)_2][PF_6]_3$ was efficiently synthesized from $[V(CH_3CN)_6][BPh_4]_2$ and ddpd[46] followed by oxidation with ferrocenium hexafluorophosphate (Figure 1a). Full characterization is collected in the Supporting Information, Figures S2 – S5. The starting vanadium material $VCl_3(CH_3CN)_3$ was checked for chromium trace impurities by ICP-MS yielding (4.01±0.31) μg g^{-1} Cr, assuring that emission from conceivable luminescent chromium(III) species will not interfere. The deuterated complex $[V([D_{17}]$-ddpd)$_2][PF_6]_3$ was prepared from $[D_{17}]$-ddpd in an analogous manner with a total degree of deuteration of 93.6 %D in the ligand and in the complex according to ESI$^+$ mass spectrometry (Supporting Information,

Figures S6 – S9). Importantly, the α-protons, closest to the vanadium center, are almost quantitatively substituted by deuterium (99 % by ^{1}H NMR spectroscopy).

The vanadium(III) oxidation state in *mer*-[V(ddpd)$_2$][PF$_6$]$_3$ was confirmed by elemental analysis, mass spectrometry, magnetometry, cyclic voltammetry and single crystal X-ray diffraction analysis (Figure 1b and Supporting Information, Figures S4 – S5, Table S1). The magnetic moment of [V(ddpd)$_2$][PF$_6$]$_3$ between 300 and 50 K amounts to $\chi T \approx 1.0$ cm^3 K mol^{-1} as expected for an $S = 1$ ground state. Below 50 K, the magnetic moment decreases due to zero-field splitting. The low temperature part was modeled with $g = 1.946$ and a zero-field splitting of $D_{exp} = +2.87(11)$ cm^{-1} (Supporting Information, Figure S4).[47,48] The vanadium(III) complex is reversibly reduced at −0.275 V vs. ferrocene (Supporting Information, Figure S5). In the solid state, the central ion in [V(ddpd)$_2$]$^{3+}$ is coordinated by six pyridine donors. The [VN$_6$] coordination geometry is nearly octahedral as shown by the octahedral shape parameter being quite close to zero (S(OC-6) = 0.63; Supporting Information, Tables S1 – S2). The [VN$_6$] symmetry is, however, less perfect than in [Cr^{III}(ddpd)$_2$]$^{3+}$ complexes (S(OC-6) = 0.29 – 0.43[46]), as a consequence of the Jahn-Teller active partially filled t$_{2g}$ shell. Compared to the metrics of the *cis-fac*-[V(ddpd)$_2$]$^{3+}$ isomer, the V-N bond lengths to the four terminal pyridines in *mer*-[V(ddpd)$_2$]$^{3+}$ decreased by 0.025 – 0.053(9) Å, while V-N distances to the central pyridines increased only slightly by 0.008/0.022(8) Å.[46] The overall smaller [VN$_6$] coordination cage of *mer*-[V(ddpd)$_2$]$^{3+}$ and its close-to-octahedral symmetry imposes the desired large ligand field splitting Δ_o.
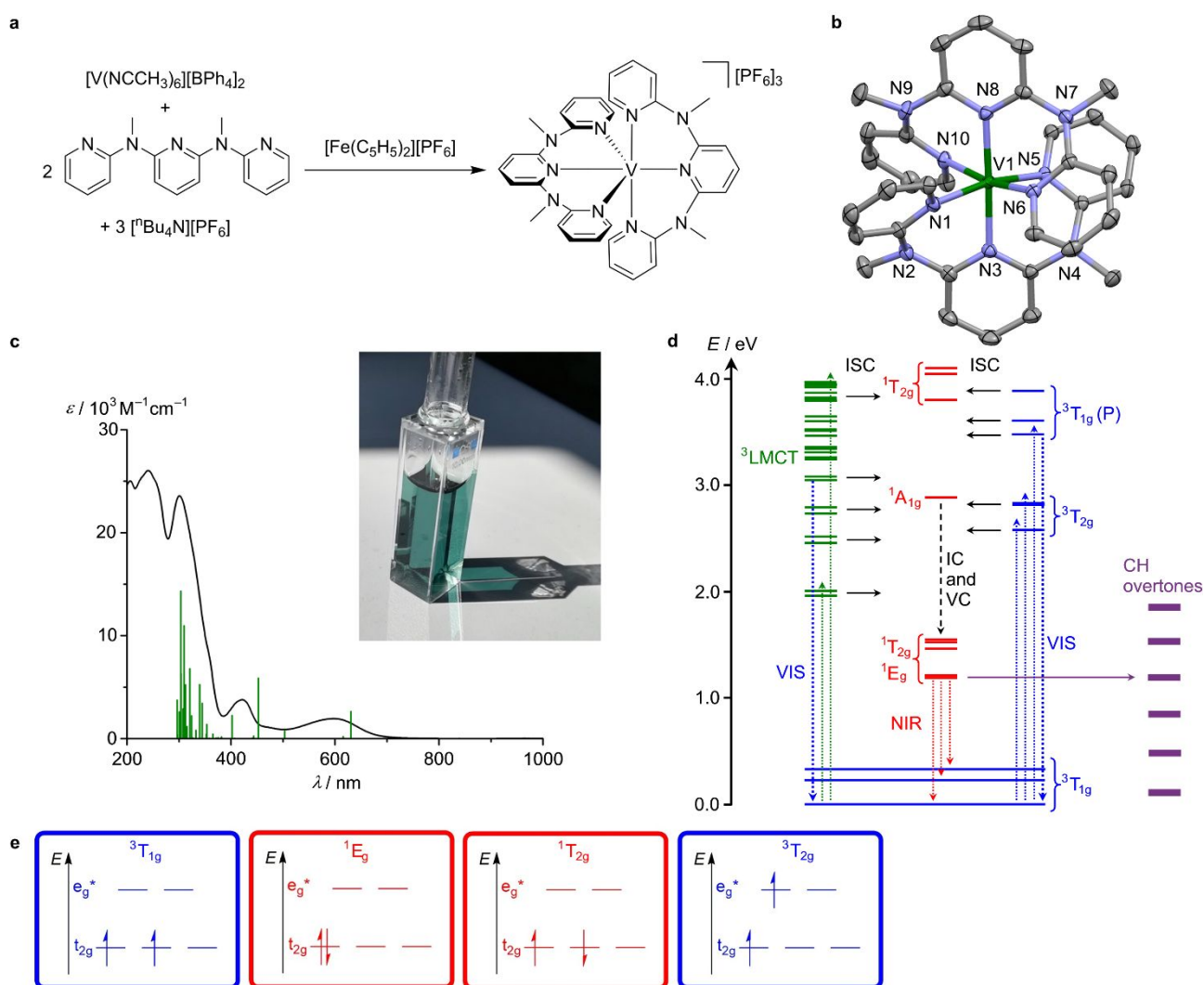

Figure 1. Synthesis, molecular structure, absorption spectrum of [V(ddpd)$_2$][PF$_6$]$_3$ and Jablonski diagram of [V(ddpd)$_2$]$^{3+}$. (a) Preparation of [V(ddpd)$_2$][PF$_6$]$_3$. (b) Molecular structure of the cation of [V(ddpd)$_2$][PF$_6$]$_3$x3 CH$_3$CN. Thermal ellipsoids are shown at 50 % probability. Hydrogen atoms, counter ions and CH$_3$CN molecules

are omitted for clarity. (c) Absorption spectrum and photograph of $[V(ddpd)_2][PF_6]_3$ in CH_3CN. The vertical green bars correspond to spin-allowed transitions calculated by TD-DFT-UKS calculations (unshifted). (d) Jablonski diagram constructed from TD-DFT-UKS (^{3}LMCT states in green) and CASSCF-NEVPT2 calculations (^{3}MC states in blue; ^{1}MC states in red); notation of MC states according to O_h symmetry; ISC = intersystem crossing; IC = internal conversion; VC = vibrational cooling; NIR = NIR emission; VIS = emission in the visible spectral region; CH overtones = multiphonon relaxation (experimental overtone energies from ref. 13). (e) Representative microstates of the most relevant metal-centered triplet and singlet states.

The electronic absorption spectrum of *mer*-$[V(ddpd)_2][PF_6]_3$ in CH_3CN reveals a broad absorption band around 597 nm (Gaussian deconvolution: 616, 570 nm), a shoulder at ~475 nm, an asymmetric band at 422 nm (Gaussian deconvolution: 429, 412 nm) and very intense bands at 301 nm (Figure 1c; Supporting Information, Figure S10). All bands are quite intense ($\varepsilon \gg 1000$ M^{-1} cm^{-1}) compared to typical metal-centered transitions, suggesting significant CT character. These intense CT bands conceal the weaker Laporte-forbidden d-d transitions, preventing their observation and hence experimental determination of Δ_o. To assign the absorption bands and to obtain the excited state level ordering including the MC states, quantum chemical calculations were performed (Supporting Information, Tables S1 – S4).

Static Quantum Chemical Calculations.

The overall geometry of $[V(ddpd)_2]^{3+}$ is well reproduced by unrestricted Kohn-Sham Density Functional Theory (DFT-UKS) calculations (CPCM(acetonitrile)-RIJCOSX-UB3LYP-D3BJ-ZORA/def2-TZVPP) with a maximum deviation in V-N bond lengths of 0.028 Å and N-V-N bond angles of 1.3° (Supporting Information, Table S1; octahedral shape parameter S(OC-6) = 0.68). Mulliken spin population analysis yields 2.07 at the vanadium center, similar to that calculated for $[V(bpy)_3]^{3+}$ (2.11),[47] accounting for the two unpaired electrons.

To assign the intense CT bands, time-dependent DFT-UKS calculations at the same level of theory were employed (Supporting Information, Table S3 – S4; Figure 1c). The absorption band at 597 nm corresponds to ^{3}LMCT transitions from the bridging nitrogen atoms to vanadium (calcd. 631/616 nm; Figures 1c, 1d). The shoulder and bands between 500 and 390 nm originate from ^{3}LMCT transitions as well (calcd. 503, 453, 444 nm; Figures 1c, 1d). The $^3T_{1g} \rightarrow {}^3T_{2g}$ ligand field transition (in octahedral symmetry) is split due to the lower symmetry (calcd. 441 and 413 nm) and superimposed onto the stronger ^{3}LMCT bands in this spectral region (Figure 1c). Compared to vanadium(III) complexes with oxygen donor ligands, e.g. $V(acac)_3$,[37-41,48] the ligand field splitting of $[V(ddpd)_2]^{3+}$ ($\Delta_o \approx 23440$ cm^{-1}) is larger by more than 2500 cm^{-1} confirming our conceptual approach of using ddpd as strong ligand to prevent back-ISC.[46]

Expectedly, the $^3T_{1g}$ ground state splits as well, yet the TD-DFT-UKS calculated energy gaps are unreasonably large (Supporting Information, Table S3). To better describe the MC triplet and singlet states (Figure 1e) and the ground state splitting, complete-active-space self-consistent field (CASSCF) calculations including spin-orbit coupling (SOC) in conjunction with fully internally contracted N-electron valence perturbation theory to second order (FIC-NEVPT2) SOC-CASSCF(6,12)-FIC-NEVPT2 on optimized $[V(ddpd)_2]^{3+}$ were performed (Supporting Information, Tables S5 – S6, Figure S11).[39,48] Figure 1d depicts the calculated order of these MC triplet and singlet states derived from CASSCF-NEVPT2 and the ^{3}LMCT states derived from TD-DFT-UKS calculations. The $^3T_{1g}$ ground state splits with $\Delta E = 1873$ and 2687 cm^{-1}, the lowest excited triplet state $^3T_{2g}$ splits into 20844, 22706, 22803 cm^{-1}. The zero-field splitting was calculated as $D_{calcd} = +6.8$ cm^{-1}, larger than the experimental value $D_{exp} = +2.87(11)$ cm^{-1}, yet similar to the experimental and calculated data of $V(acac)_3$ ($D_{exp} = +6.9$ cm^{-1}; $D_{calcd} = +9.6$ cm^{-1}).[48]

A series of five singlet states originating from the $^1T_{2g}$ and ^1E_g terms is located between the triplet ground and excited states. This excited state ordering confirms the large ligand field splitting with $\Delta_o > 17.3$ *B*. The two lowest singlet states centered at 9612 and 9736 cm^{-1} (Supporting Information, Figure S11) are only weakly split by $\Delta E = 124$ cm^{-1}. A sixth (isolated) singlet state ($^1A_{1g}$) is predicted at 23283 cm^{-1}, slightly above the highest level of the $^3T_{2g}$ states by 480 cm^{-1}. This calculation suggests that Δ_o is slightly smaller than 36.6 *B* (in

a standard Tanabe-Sugano diagram with *C*/*B* = 4.42, Supporting Information, Figure S1). The combined TD-DFT-UKS and CASSCF-NEVPT2 calculations indicate that several states (^{3}LMCT, $^3T_{2g}$ and $^1A_{1g}$) lie in the 3.1 – 2.6 eV (400 – 480 nm) region.

Steady-state and Time-resolved Spectroscopy.

Steady-state emission spectra with excitation at 306 nm (4.05 eV) at 77 K in a valeronitrile glass matrix show rich spectral features between 370 and 1150 nm (Figure 2a). Obviously, several states are emissive upon high-energy excitation. The NIR-II emission is also observed in butyronitrile glass at 10 K with excitation wavelengths between 306 and 450 nm. The highest intensity occurs at an excitation wavelength of 360 nm, where the luminescence is twice as strong as at 306 nm excitation, while the luminescence almost vanishes when exciting with 450 nm (Figure 2c). Tuning the excitation wavelength populates different electronically excited triplet states which might exhibit different ISC efficiencies as sketched in Figure 1d and consequently lead to different phosphorescence intensities. In the solid state (KBr pellet; Supporting Information, Figures S14a, S14b) the NIR-II emission is not observed, probably resulting from self-quenching. The emission in solution is sensitive to the presence of oxygen. A biexponential lifetime of several hundred nanoseconds is associated with the sharp NIR emission bands at 1100 nm (790 ns (93 %), 8800 ns (7 %), Supporting Information, Table S7, Figure S12). The long lifetime is in a similar range compared to the excited singlet state lifetime reported for V^{3+} doped in NaMgAl(ox)$_3$ at 11 K (τ < 500 ns).[41] All emission bands show vibrational progression, while the ground state splitting might also account for the observed pattern.
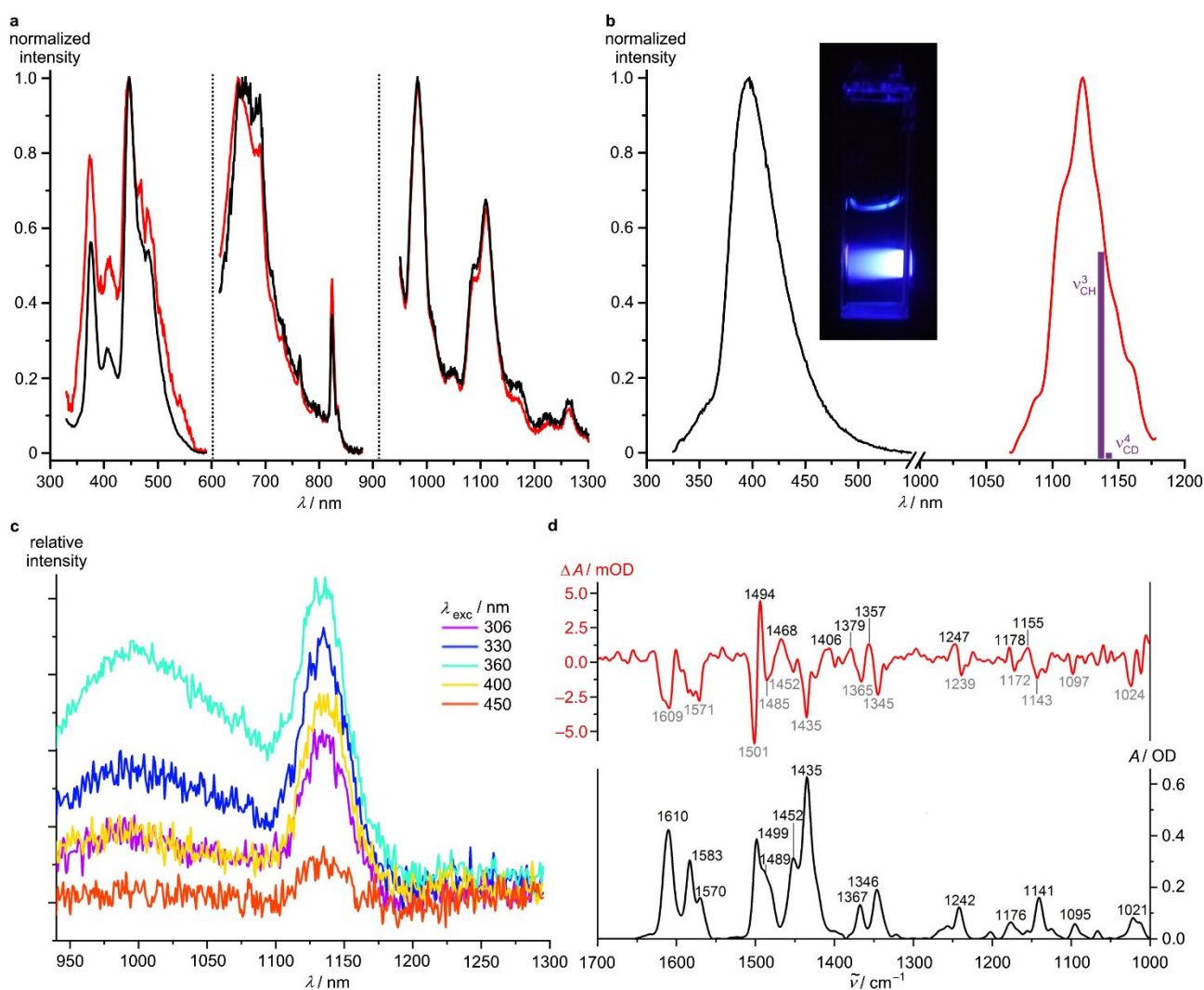
Figure 2. (a) Normalized luminescence spectra of $[V(ddpd)_2][PF_6]_3$ (black) and $[V([D_{17}]\text{-}ddpd)_2][PF_6]_3$ (red) (λ_{exc} = 306 nm, ^nBuCN, 77 K). Intensities in the different spectral regions are not to scale due to different detectors and gratings used. GG455 and RG850 long pass filters were employed for the low-energy spectra, respectively. (b) Normalized luminescence spectra of $[V(ddpd)_2][PF_6]_3$ (λ_{exc} = 306 nm, CD_3CN, 298 K). Intensities in the different spectral regions are not to scale due to different detectors and gratings used. The integral ratio of the two bands amounts to $I(VIS) : I(NIR) = 2.1 : 1.8\times10^{-4}$. Purple vertical bars indicate relevant CH and CD overtones. Their length approximately illustrates the $\nu^3_{CH} : \nu^4_{CD}$ intensity ratio.[13] The photograph illustrates the blue fluorescence of $[V(ddpd)_2][PF_6]_3$ (λ_{exc} = 350 nm, CH_3CN, 298 K). (c) Luminescence spectra of $[V(ddpd)_2][PF_6]_3$ (λ_{exc} = 306 – 450 nm, butyronitrile glass, 20 K). (d) Ground-state FTIR (black) and step-scan FTIR spectrum (red) of $[V(ddpd)_2][PF_6]_3$ at 20 K (λ_{exc} = 355 nm, KBr pellet, 0 – 300 ns).

Based on the quantum chemical calculations (Figure 1d), the emission energies and the lifetimes (Supporting Information, Figures S12 – S13, Table S7), we assign the high-energy emission bands (374, 447 and 660 nm) and the NIR-I/NIR-II emission bands (982 and 1088/1109 nm) to fluorescence and phosphorescence, respectively. The NIR-I and NIR-II phosphorescence originates from the two almost degenerate lowest excited singlet states (with ^1E_g and $^1T_{2g}$ parentage) decaying radiatively to the split ground state levels (Figure 1d). From these NIR-I/NIR-II phosphorescence bands, the experimental ground state splitting is estimated as 1080 cm^{-1} (averaged 1088/1109 nm), which is somewhat smaller than that obtained by the CASSCF-NEVPT2 calculations (1873 cm^{-1}; Figure 1d). As a reference, a splitting of 880 cm^{-1} was calculated for $V(acac)_3$ by SOC-CASSCF(12,10)-NEVPT2,[48] while a value of 1400 cm^{-1} was experimentally determined for $[V(urea)_6][ClO_4]_3$.[40] Excitation of ^3LMCT states at lower energy (600 nm) does not lead to the NIR-II luminescence, demonstrating that these ^3LMCT states do not efficiently evolve to the emissive singlet states (Figure 1d).

In diluted deaerated CD_3CN solution, dual emission at 396 and 1109/1123 nm occurs even at 298 K upon excitation at 306 nm (Figure 2b). The high-energy blue emission is even observable by the naked eye at room temperature in solution and in a KBr pellet (Figure 2b; Supporting Information, Figure S14c). The quantum yield of the high energy fluorescence is very high with Φ = 2.1 % and surpasses the quantum yield of the blue emission of the recently reported blue emissive cobalt(III) complexes (Φ = 0.7/0.4 %).[8] The emission decay at 396 nm is biexponential with τ_{396} of 3.2 (56 %) and 8.2 (44 %) ns and 1.7 (51 %) and 6.3 (49 %) ns at 298 K and 77 K. respectively. We assign this fluorescence to $^3T_{1g}(P)\rightarrow{}^3T_{1g}$ or to ^3LMCT transitions (Figure 1d). Indeed, two ^3LMCT states are calculated around 3 eV by TD-DFT calculations and $^3T_{2g}(P)$ states around 3.46 eV by CASSCF-NEVPT2 calculations, which could account for the biexponential decay as sketched in Figure 1d with blue vertical arrows (Supporting Information, Tables S3 and S6).

Beyond the intense blue emission of $[V(ddpd)_2][PF_6]_3$, the observed room temperature NIR-II phosphorescence of $[V(ddpd)_2][PF_6]_3$ in solution is unique. The NIR quantum yield of Φ = 1.8×10^{-4} % is not very high but the rather sharp emission band (FWHM ca. 325 cm^{-1}) is clearly observable. To the best of our knowledge, no other complexes with Earth-abundant metal ions display NIR-II luminescence in frozen and in fluid solution (Figures 2a – 2c). The ground state splitting of the $^3T_{1g}$ levels (Figure 1d) rather than vibrational progression likely accounts for the asymmetric band shape. This differs from NIR emission bands of chromium(III) complexes, which possess an orbitally non-degenerate ground state ($^4A_2$) and consequently deliver sharp phosphorescence bands.[12-17]

In order to obtain information on the long-lived excited singlet states, the complex (in a KBr pellet) was excited with 355 nm at 20 K and probed by step-scan FT-IR spectroscopy. The measured FTIR ground state spectrum is in excellent agreement with the DFT-UKS calculated spectrum of $[V(ddpd)_2]^{3+}$ (Supporting Information, Figure S15). The recorded step-scan difference spectrum collected between 0 and 300 ns after the pulse shows the ground state bleach (negative bands) and excited state absorption (positive bands) (Figure 2d). The latter vibrational bands correspond to the lowest energy long-lived singlet state. A monoexponential lifetime of about 290 ns was determined by performing a global exponential fit for the most prominent positive and negative peaks in the step-scan difference spectrum (Supporting Information,

7

Figure S16). The observation of step-scan FTIR spectra further confirm the presence of long-lived excited states.

The lifetime of this emissive excited state depends on the efficiency of non-radiative decay processes. Especially, NIR luminescence is prone to multiphonon relaxation via CH overtones which could be diminished by deuteration.[13,32,33] Indeed, the second aromatic CH overtone (ν^3_{CH} = 8972 cm^{-1} as estimated from CH overtone IR spectroscopy of 6,6'-dimethyl-2,2'-bipyridine)[13] has a significant spectral overlap with the NIR-II emission bands of [V(ddpd)$_2$][PF$_6$]$_3$ (Figure 2b). For the deuterated derivative, the third CD overtone at ν^4_{CD} = 8755 cm^{-1} is the most relevant one (Figure 2b).[13] Due to the lower energy and lower extinction coefficient of the third CD overtone ν^4_{CD}, the spectral overlap with the vanadium NIR-II emission band should be smaller. Consequently, the non-radiative rate constant for the deuterated complex should be smaller than for the protio derivative. As long as this multiphonon pathway dominates the decay of the singlet states, the NIR quantum yield and lifetime of [V([D$_{17}$]-ddpd)$_2$]$^{3+}$ should be larger than those of [V(ddpd)$_2$]$^{3+}$. However, within experimental uncertainty, we cannot observe significant differences between the NIR emission intensities and lifetimes of [V([D$_{17}$]-ddpd)$_2$]$^{3+}$ and [V(ddpd)$_2$]$^{3+}$ at 298 K and 77 K (Supporting Information, Figures S12 – S13 and S17 – S18, Table S7). This suggests that other non-radiative pathways dominate the decay of the lowest energy singlet states in [V(ddpd)$_2$]$^{3+}$. Presumably, the split ground state levels favor ISC to the ground state (Figure 1d).

The dual emission of [V(ddpd)$_2$][PF$_6$]$_3$ in the blue and NIR-II spectral region demonstrates the huge energy difference of ca. 2 eV between these two luminescent states. The observed intense fluorescence of [V(ddpd)$_2$]$^{3+}$ suggests that the ISC rates from the triplets to the singlets are not particularly large. This slow ISC then opens other pathways (fluorescence, non-radiative decay from the triplets) before the singlet states are populated to higher extents.

The initial dynamics was then probed by fs-transient absorption (TA) spectroscopy. TA spectra of [V(ddpd)$_2$][PF$_6$]$_3$ in CH$_3$CN recorded after excitation with femtosecond laser pulses at 620 nm (~2 eV) show excited state absorptions (ESA) at around 500 and 670 nm (Supporting Information, Figure S19). With a time constant of 6.3 ps the ground state is essentially recovered. Hence, the ^{3}LMCT states do not significantly evolve to the emissive singlets as already demonstrated by the steady-state luminescence data. This is consistent with the assumption that efficient ISC requires a high density of final states in the energy region of interest.[45] Around 2 eV, such singlet states are unavailable for [V^{III}(ddpd)$_2$]$^{3+}$ (Figure 1d). However, a singlet state is present at higher energy (^{1}A$_{1g}$, 2.89 eV from the CASSCF-NEVPT2 calculation; Figure 1d).

TA spectra recorded after excitation at 400 nm (3.1 eV; ^{3}LMCT and ^{3}T$_{2g}$ states) exhibit a dominant ultrafast decay to the ground state with a time constant of 4.9 ps and a second weaker time constant of 74 ps (Figure 3, Supporting Information, Figure S20). On the nanosecond time scale, a small component persists showing an excited state absorption around 460 nm (Figures 3c and 3d). We assign this component to the long-lived singlet state(s), similar to the analogous amplitude spectrum of [Cr(ddpd)$_2$]$^{3+}$, representing its emissive doublet states, at longer times scales (Figure 3d).[49] These results agree with the observation, that a small fraction of the triplet population evolves to the singlet states via ISC. Obviously, the low-energy ^{3}LMCT states are less competent to feed the spin-flip singlet states than the ^{3}T$_{2g}$ and higher energy ^{3}LMCT states. Conceptually, the energy tuning of ^{3}LMCT and ^{3}T$_{2g}$ states as well as identification of suitable antenna systems should enable an even more efficient population of the emissive singlet states of vanadium(III) complexes.
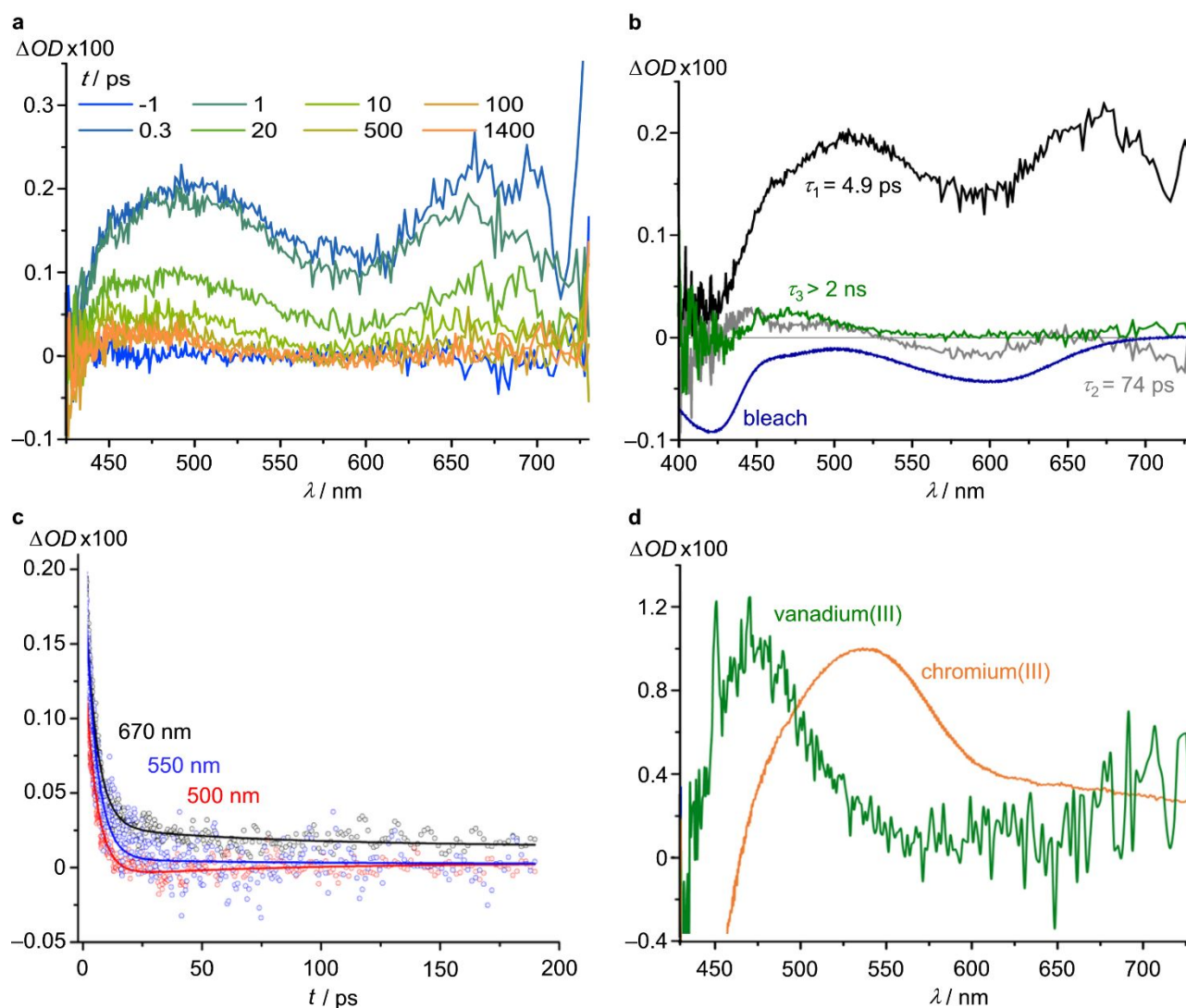
Figure 3. fs-Transient absorption spectroscopy of [V(ddpd)$_2$][PF$_6$]$_3$. (a) Transient absorption spectra of [V(ddpd)$_2$][PF$_6$]$_3$ in CH$_3$CN excited with 400 nm laser pulses. (b) Bleach (blue) and decay associated amplitude spectra labelled with the corresponding time constants: τ_1 = 4.9 ps (~70 %, black), τ_2 = 74 ps (~20 %, grey) and long-living component with a time constant τ_3 > 2 ns (~10 %, green). (c) Transient signals as a function of the pump–probe delay time observed at 670 nm (black), 550 nm (blue) and 500 nm (red). The fits to the experimental data correspond to triexponential decays with $\tau_{1,2}$ = 4.9, 74 ps and a time constant τ_3 > 2 ns. (d) Scaled amplitude spectra of the long-lived components of [V(ddpd)$_2$][PF$_6$]$_3$ (green) and [Cr(ddpd)$_2$][BF$_4$]$_3$ (orange) (chromium(III) data from ref. 49).

Molecular dynamics calculations.

In order to gain deeper insight into the complex spin-flip dynamics of [V(ddpd)$_2$]$^{3+}$ after excitation, dynamics simulations starting from the ^{3}LMCT manifold in acetonitrile were performed. Specifically, non-adiabatic surface hopping including arbitrary couplings (SHARC) dynamics simulations with a linear vibronic coupling (LVC) model were employed.[50] Initially, 100 fs were propagated from the four lowest ^{3}LMCT states located at 3.5 − 3.7 eV (354 − 333 nm (Supporting Information, Table S3, Figures S21 − S22), finding one ^{3}LMCT state with a significant amount of trapped population. Subsequently and starting from this state (2^{3}LMCT) located at 3.59 eV (345 nm), we propagated during 50000 fs and observed IC to the ^{3}MC states (^{3}T$_{2g}$ and ^{3}T$_{1g}$ ground state) and ISC to a singlet state 2^{1}MC (Figure 1d, Figure 4).
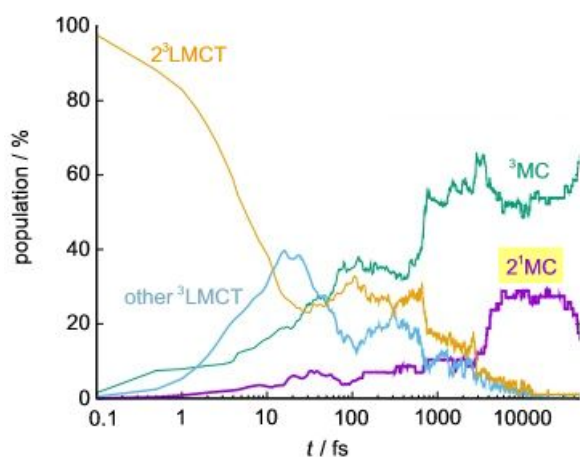
Figure 4. Time-evolution of the population of the excited states during 50000 fs (in logarithmic scale) after starting the dynamics on the 2^3LMCT state (the longest lived triplet state after 100 fs, Supporting Information, Figure S22). The label "other ^{3}LMCT" stands for the population in any other state but the 2^3LMCT. The label "^{3}MC" corresponds to the sum of populations in every triplet MC state, indicating the total amount of internal conversion. Population in any other singlet state other than 2^1MC is negligible and not plotted.

The singlet ^{1}LMCT manifold acts as a mere spectator during the dynamics. The most populated metal-centered singlet state 2^1MC was then optimized within the LVC method. The optimized geometry (Supporting Information, Table S8) lies 1.10 eV (1127 nm) above the $^3T_{1g}$ ground state, in very good agreement with the experimental emission energy, thus validating the dynamical approach. The dynamics calculations confirm that the 2^3LMCT state at high energy (3.59 eV) undergoes ISC to a singlet state of MC character while no lower energy ^{1}LMCT states around 2 eV are involved in the excited state evolution towards the emissive ^{1}MC state, as already suggested by the steady-state and time-resolved experimental data.

Conclusion

Our study extends the very series of luminescent metal complexes with Earth-abundant 3d metal ions (Cr, Fe, Co, Cu) to the early 3d transition metal vanadium. The vanadium(III) complex *mer*-[V(ddpd)$_2$]$^{3+}$ with a tuned large ligand field splitting exhibits a deep-blue emission at room temperature in solution and a long-lived phosphorescence above 1000 nm. This expands the spectral region previously accessible with 3d metal complexes (Vis and NIR-I) to the NIR-II region for the first time. Conceptual design principles for NIR-II luminescent vanadium(III) complexes evolved, highlighting the distinct roles of ligand-to-metal charge transfer states, intersystem crossing and multiphonon relaxation. This first success in designing blue and NIR-II emissive complexes of the Earth-abundant metal vanadium raises the prospect of employing luminescent vanadium complexes in the future. Especially, dual emissive complexes could find applications as optical probes with a built-in internal reference for chemical or physical perturbations. Work in this direction is currently in progress.

ASSOCIATED CONTENT

Supporting Information

Data of quantum chemical calculations, synthetic procedures, analytical and spectroscopic data of [V(ddpd)$_2$][PF$_6$]$_3$. This material is available free of charge via the Internet at http://pubs.acs.org.

AUTHOR INFORMATION

Corresponding Authors

* katja.heinze@uni-mainz.de (ORCID 0000-0003-1483-4156), gerhards@chemie.uni-kl.de (ORCID 0000-0002-8748-2940), michael.seitz@uni-tuebingen.de (ORCID 0000-0002-9313-2779).

Notes
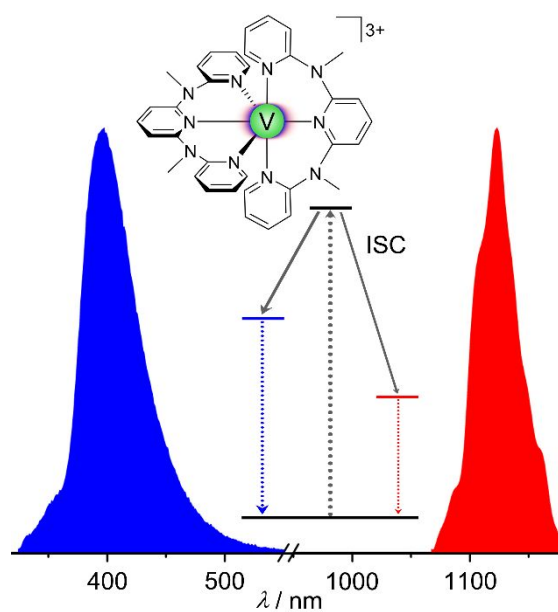
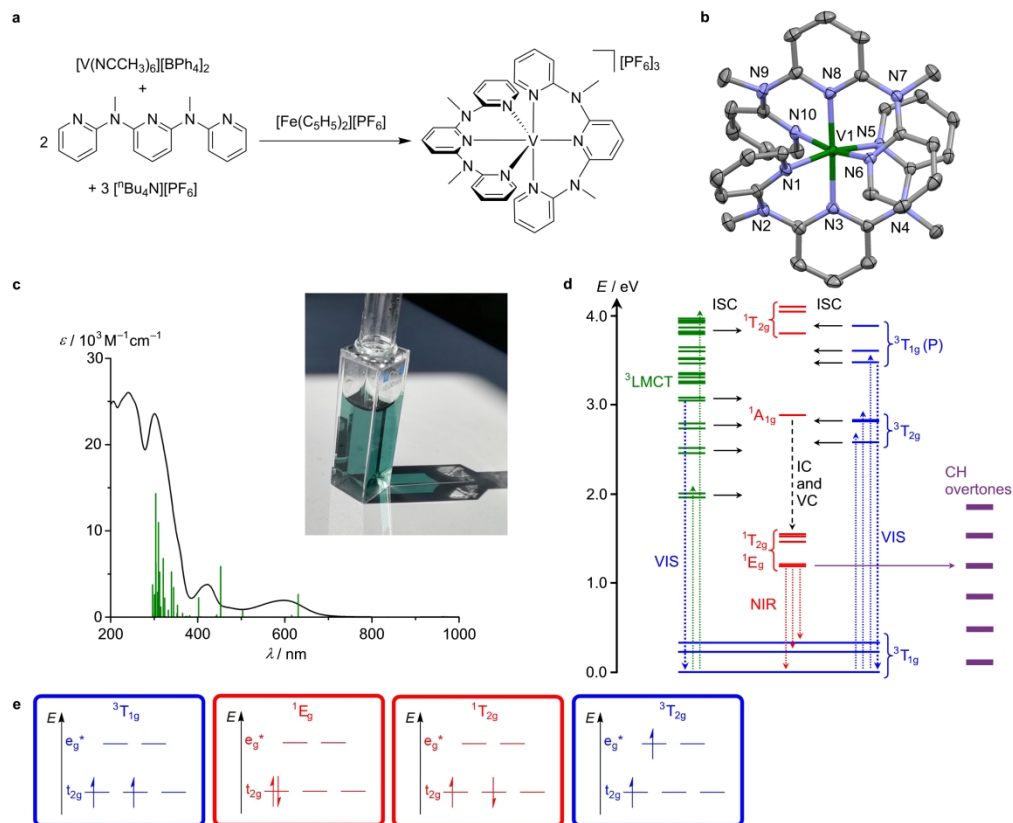The authors declare no competing financial interest.

REFERENCES

(1) a) Wenger, O. S. Photoactive Complexes with Earth-Abundant Metals. *J. Am. Chem. Soc.* **2018**, *140*, 13522–13533; b) Förster, C.; Heinze, K. Photophysics and photochemistry with Earth-abundant metals – fundamentals and concepts. *Chem. Soc. Rev.* **2020**, *49*, 1057–1070.

(2) Otto, S.; Dorn, M.; Förster, C.; Bauer, M.; Seitz, M.; Heinze, K. Understanding and Exploiting Long-lived Near-infrared Emission of a Molecular Ruby. *Coord. Chem. Rev.* **2018**, *359*, 102–111.

(3) Bizzarria, C.; Spuling, E.; Knoll , D. M.; Volz, D.; Bräse, S. Sustainable metal complexes for organic light-emitting diodes (OLEDs). *Coord. Chem. Rev.* **2018**, *373*, 49–82.

(4) McCusker, J. K. Electronic structure in the transition metal block and its implications for light harvesting. *Science* **2019**, *363*, 484–488.

(5) Wagenknecht, P. S.; Ford, P. C. Metal centered ligand field excited states: Their roles in the design and performance of transition metal based photochemical molecular devices. *Coord. Chem. Rev.* **2011**, *255*, 591–616.

(6) Zhang, W.; Alonso-Mori, R.; Bergmann, U.; Bressler, C.; Chollet, M.; Galler, A.; Gawelda, W.; Hadt, R. G.; Hartsock, R. W.; Kroll, T.; Kjær, K. S.; Kubiček, K.; Lemke, H. T.; Liang, H. W.; Meyer, D. A.; Nielsen, M. M.; Purser, C.; Robinson, J. S.; Solomon, E. I.; Sun, Z.; Sokaras, D.; van Driel, T. B.; Vankó, G.; Weng, T. C.; Zhu, D.; Gaffney, K. J. Tracking excited-state charge and spin dynamics in iron coordination complexes. *Nature* **2014**, *15*, 345–348.

(7) Büldt, L. A.; Guo, X.; Vogel, R.; Prescimone, A.; Wenger, O. S. A Tris(diisocyanide)chromium(0) Complex Is a Luminescent Analog of $Fe(2,2'\text{-Bipyridine})_3^{2+}$. *J. Am. Chem. Soc.* **2017**, *139*, 985–992.

(8) Pal, A. K.; Li, C.; Hanan, G. S.; Zysman-Colman, E. Blue-Emissive Cobalt(III) Complexes and Their Use in the Photocatalytic Trifluoromethylation of Polycyclic Aromatic Hydrocarbons. *Angew. Chem. Int. Ed.* **2018**, *57*, 8027–8031.

(9) Chábera, P.; Liu, Y.; Prakash, O.; Thyrhaug, E.; El Nahhas, A.; Honarfar, A.; Essén, S.; Fredin, L. A.; Harlang, T. C. B.; Kjær, K. S.; Handrup, K.; Ericson, F.; Tatsuno, H.; Morgan, K.; Schnadt, J.; Häggström, L.; Ericsson, T.; Sobkowiak, A.; Lidin, S.; Huang, P.; Styring, S.; Uhlig, J.; Bendix, J.; Lomoth, R.; Sundström, V.; Persson, P.; Wärnmark, K. A low-spin Fe(III) complex with 100-ps ligand-to-metal charge transfer photoluminescence. *Nature* **2017**, *543*, 695–699.

(10) Kjær, K. S.; Kaul, N.; Prakash, O.; Chábera, P.; Rosemann, N. W.; Honarfar, A.; Gordivska, O.; Fredin, L. A.; Bergquist, K.-E.; Häggström, L.; Ericsson, T.; Lindh, L.; Yartsev, A.; Styring, S.; Huang, P.; Uhlig, J.; Bendix, J.; Strand, D.; Sundström, V.; Persson, P.; Lomoth, R.; Wärnmark, K. Luminescence and reactivity of a charge-transfer excited iron complex with nanosecond lifetime. *Science* **2019**, *363*, 249–253.

(11) Hamze, R.; Peltier, J. L.; Sylvinson, D.; Jung, M.; Cardenas, J.; Haiges, R.; Soleilhavoup, M.; Jazzar, R.; Djurovich, P. I.; Bertrand, G.; Thompson, M. E. Eliminating nonradiative decay in Cu(I) emitters: >99% quantum efficiency and microsecond lifetime. *Science* **2019**, *36*, 601–606.

(12) Otto, S.; Grabolle, M.; Förster, C.; Kreitner, C.; Resch-Genger, U.; Heinze, K. $[Cr(ddpd)_2]^{3+}$: A molecular, water-soluble, highly NIR-emissive ruby analogue. *Angew. Chem. Int. Ed.* **2015**, *54*, 11572–11576.

(13) Wang, C.; Otto, S.; Dorn, M.; Kreidt, E.; Lebon, J.; Sršan, L.; Di Martino-Fumo, P.; Gerhards, M.; Resch-Genger, U.; Seitz, M.; Heinze, K. Deuterated Molecular Ruby with Record Luminescence Quantum Yield. *Angew. Chem. Int. Ed.* **2018**, *57*, 1112–1116.

(14) Otto, S.; Förster, C.; Wang, C.; Resch-Genger, U.; Heinze, K. A strongly luminescent chromium(III) complex acid. *Chem. Eur. J.* **2018**, *24*, 12555–12563.

(15) Otto, S.; Harris, J.; Heinze, K.; Reber, C. Molecular ruby under pressure. *Angew. Chem. Int. Ed.* **2018**, *57*, 11069–11073.

(16) Treiling, S.; Wang, C.; Förster, C.; Reichenauer, F.; Kalmbach, J.; Boden, P.; Harris, J. P.; Carrella, L. M.; Rentschler, E.; Resch-Genger, U.; Reber, C.; Seitz, M.; Gerhards, M.; Heinze, K. Luminescence and Light-driven Energy and Electron Transfer from an Exceptionally Long-lived Excited State of a Non-innocent Chromium(III) Complex. *Angew. Chem Int. Ed.* **2019**, *58*, 18075–18085.

(17) a) Jiménez, J. R.; Doistau, B.; Cruz, C. M.; Besnard, C.; Cuerva, J. M.; Campaña, A. G.; Piguet, C. Chiral Molecular Ruby [Cr(dqp)$_2$]$^{3+}$ with Long-Lived Circularly Polarized Luminescence. *J. Am. Chem. Soc.* **2019**, *141*, 13244–13252; b) Dee, C.; Zinna, F.; Kitzmann, W. R.; Pescitelli, G.; Heinze, K.; Di Bari, L.; Seitz, M. Strong Circularly Polarized Luminescence of an Octahedral Chromium(III) Complex. *Chem. Commun.* **2019**, *55*, 13078–13081.

(18) a) Bünzli, J.-C. G.; Eliseeva, S. V. Lanthanide NIR luminescence for telecommunications, bioanalyses and solar energy conversion. *J. Rare Earths* **2010**, *28*, 824–842; b) Bünzli, J.-C. G. Lanthanide light for biology and medical diagnosis. *J. Lumin.* **2016**, *170*, 866–878.

(19) Ibrahim-Ouali, M.; Dumur, F. Recent Advances on Metal-Based Near-Infrared and Infrared Emitting OLEDs. *Molecules* **2019**, 24, 1412.

(20) Ye, H. Q.; Li, Z.; Peng, Y.; Wang, C. C.; Li, T. Y.; Zheng, Y. X.; Sapelkin, A.; Adamopoulos, G.; Hernández, I.; Wyatt, P. B.; Gillin, W. P. Organo-erbium systems for optical amplification at telecommunications wavelengths. *Nat. Mater.* **2014**, *13*, 382–386.

(21) Carlos, L. D.; Ferreira, R. A. S.; Bermudez, V. d. Z.; Ribeiro, S. J. L. Lanthanide-Containing Light-Emitting Organic–Inorganic Hybrids: A Bet on the Future. *Adv. Mater.* **2009**, *21*, 509–534.

(22) Foucault-Collet, A.; Gogick, K. A.; White, K. A.; Villette, S.; Pallier, A.; Collet, G.; Kieda, C.; Li, T.; Geib, S. J.; Rosi, N. L.; Petoud, S. Lanthanide near infrared imaging in living cells with Yb^{3+} nano metal organic frameworks. *Proc. Natl. Acad. Sci. U. S. A.* **2013**, *110*, 17199–17204.

(23) Yang, Q.; Hu, Z.; Zhu, S.; Ma, R.; Ma, H.; Ma, Z.; Wan, H.; Zhu, T.; Jiang, Z.; Liu, W.; Jiao, L.; Sun, H.; Liang, Y.; Dai, H., Donor Engineering for NIR-II Molecular Fluorophores with Enhanced Fluorescent Performance. *J. Am. Chem. Soc.* **2018**, *140*, 1715–1724.

(24) Cai, Y.; Wei, Z.; Song, C.; Tang, C.; Han, W.; Dong, X. Optical nano-agents in the second near-infrared window for biomedical applications. *Chem. Soc. Rev.* **2019**, *48*, 22–37.

(25) Zhang, M.; Zheng, W.; Liu, Y.; Huang, P.; Gong, Z.; Wei, J.; Gao, Y.; Zhou, S.; Li, X.; Chen, X. A New Class of Blue-LED-Excitable NIR-II Luminescent Nanoprobes Based on Lanthanide-Doped CaS Nanoparticles. *Angew. Chem. Int. Ed.* **2019**, *58*, 9556–9560.

(26) Zhu, S.; Yung, B. C.; Chandra, S.; Niu, G.; Antaris, A. L.; Chen, X. Near-Infrared-II (NIR-II) Bioimaging via Off-Peak NIR-I Fluorescence Emission *Theranostics* **2018**, *8*, 4141–4151.

(27) Wang, P.; Fan, Y.; Lu, L.; Liu, L.; Fan, L.; Zhao, M.; Xie, Y.; Xu, C.; Zhang, F. NIR-II nanoprobes in-vivo assembly to improve image-guided surgery for metastatic ovarian cancer. *Nat. Commun.* **2018**, *9*, 2898.

(28) Schulze, M.; Steffen, A.; Würthner, F. Near-IR Phosphorescent Ruthenium(II) and Iridium(III) Perylene Bisimide Metal Complexes. *Angew. Chem. Int. Ed.* **2015**, *54*, 1570–1573.

(29) Bünzli, J.-C. G.; Eliseeva, S. V. Basics of Lanthanide Photophysics. in Lanthanide Luminescence: Photophysical, Analytical and Biological Aspects. Hänninen, P.; Härmä, H. (eds.), Springer-Verlag Berlin Heidelberg (2010).

(30) Englman, R.; Jortner, J. The energy gap law for radiationless transitions in large molecules. *Mol. Phys.* **1970**, *18*, 145–164.
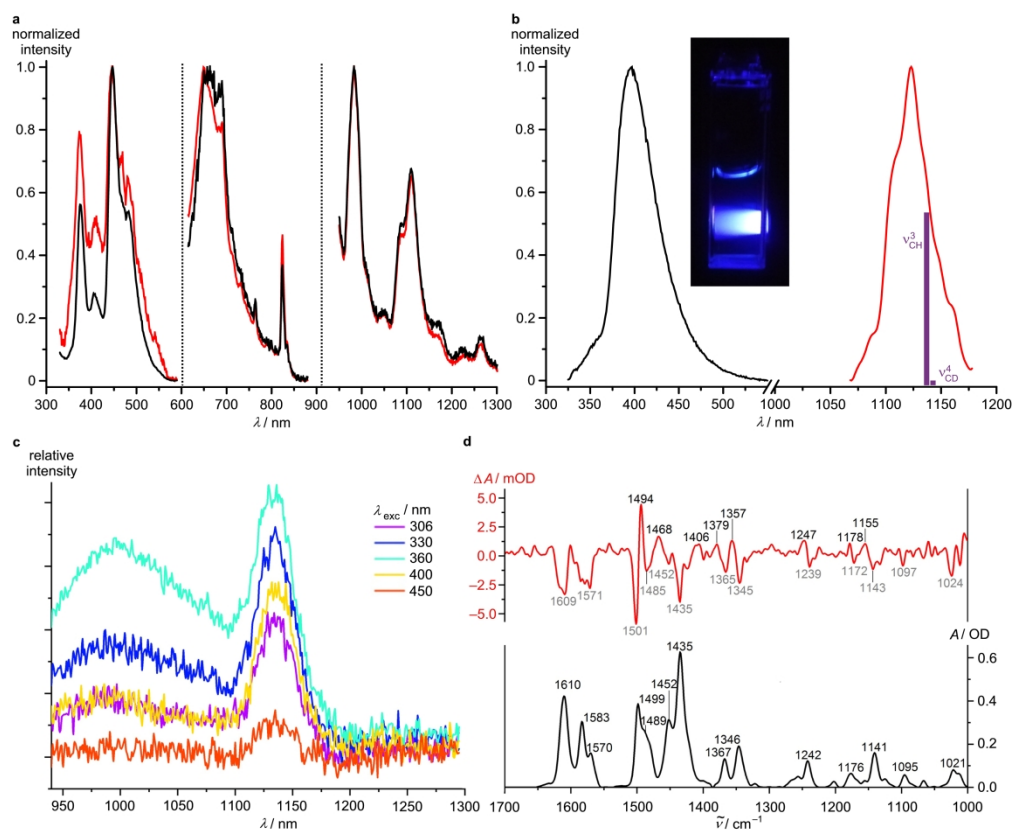
(31) Casper, J. V.; Kober, E. M.; Sullivan, B. P.; Meyer, T. J. Application of the Energy Gap Law to the Decay of Charge-Transfer Excited States. *J. Am. Chem. Soc.* **1982**, *104*, 630–632.

(32) Sveshnikova, E. B.; Ermolaev, V. L. Inductive-Resonant Theory of Nonradiative Transitions in Lanthanide and Transition Metal Ions. *Opt. Spectrosc.* **2011**, *111*, 34–50.

(33) Kreidt, E.; Kruck, C.; Seitz, M. Non-radiative Deactivation of Lanthanoid Luminescence by Multiphonon Relaxation in Molecular Complexes. Handbook on the Physics and Chemistry of Rare Earths **2018**, *53*, 35–79, Elsevier, Amsterdam.

(34) Doffek, C.; Seitz, M. The Radiative Lifetime in Near-IR-Luminescent Ytterbium Cryptates: The Key to Extremely High Quantum Yields. *Angew. Chem. Int. Ed.* **2015**, *54*, 9719–9721.

(35) Hu, J.-Y., Ning, Y., Meng, Y.-S., Zhang, J., Wu, Z.-Y., Gao, S. & Zhang, J.-L. Highly near-IR emissive ytterbium(III) complexes with unprecedented quantum yields. *Chem. Sci.* **2017**, *8*, 2702–2709.

(36) Zhang, J.-X.; Chan, W.-L.; Xie, C.; Zhou, Y.; Chau, H.-F.; Maity, P.; Harrison, G. T.; Amassian, A.; Mohammed, O. F.; Tanner, P. A.; Wong, W.-K.; Wong, K.-L. Impressive near-infrared brightness and singlet oxygen generation from strategic lanthanide–porphyrin double-decker complexes in aqueous solution. *Light-Sci. Appl.* **2019**, *8*, 46.

(37) Kittilstved, K. R.; Hauser, A. Electronic structure and photophysics of pseudo-octahedral vanadium(III) oxo complexes. *Coord. Chem. Rev.* **2010**, *254*, 2663–2676.

(38) Reber, C.; Güdel, H. U. Near Infrared Luminescence Syectrocopy of Al_2O_3:V^{3+} and YP_3O_9:V^{3+}. *Chem. Phys. Lett.* **1989**, *154*, 425–431.

(39) Landry-Hum, J.; Bussière, G.; Daniel, C.; Reber, C. Triplet Electronic States in d^2 and d^8 Complexes Probed by Absorption Spectroscopy: A CASSCF/CASPT2 Analysis of $[V(H_2O)_6]^{3+}$ and $[Ni(H_2O)_6]^{2+}$. *Inorg. Chem.* **2001**, *40*, 2595–2601.

(40) Beaulac, R.; Tregenna-Piggott, P. L. W.; Barra, A.-L. Høgni Weihe; Luneau, D.; Reber, C. The Electronic Ground State of $[V(urea)_6]^{3+}$ Probed by NIR Luminescence, Electronic Raman, and High-Field EPR Spectroscopies. *Inorg. Chem.* **2006**, *45*, 3399–3407.

(41) Kittilstved, K. R.; Hauser, Electronic structure of V^{3+} in $NaMgAl(ox)_3 \cdot 9H_2O$ probed by Fourier Transform spectroscopy. *J. Lumin.* **2009**, *129*, 1493–1496.

(42) Van Kuiken, B. E.; Hahn, A. W.; Maganas, D.; DeBeer, S. Measuring Spin-Allowed and Spin-Forbidden d−d Excitations in Vanadium Complexes with 2p3d Resonant Inelastic X-ray Scattering. *Inorg. Chem.* **2016**, *55*, 11497–11501.

(43) Reber, C.; Güdel, H. U.; Meyer, G.; Schleid, T.; Daul, C. A. Optical Spectroscopic and Structural Properties of V^{3+}-Doped Fluoride, Chloride, and Bromide Elpasolite Lattices. *Inorg. Chem.* **1989**, *28*, 3249–3258.

(44) Wenger, O. S.; Güdel, H. U. Luminescence spectroscopy of V^{3+}-doped Cs_2NaYCl_6 under high pressure. *Chem. Phys. Lett.* **2002**, *354*, 75–81.

(45) Penfold, T. J.; Gindensperger, E.; Daniel, C.; Marian, C. M. Spin-Vibronic Mechanism for Intersystem Crossing. *Chem. Rev.* **2018**, *118*, 6975–7025.

(46) Förster, C.; Dorn, M.; Reuter, T.; Otto, S.; Davarci, G.; Reich, T.; Carrella, L.; Rentschler, E.; Heinze, K. Ddpd as Expanded Terpyridine: Dramatic Effects of Symmetry and Electronic Properties in First Row Transition Metal Complexes. *Inorganics* **2018**, *6*, 86.

(47) Bowman, A. C.; Sproules, S.; Wieghardt, K. Electronic Structures of the $[V(^tbpy)_3]^z$ (z = 3+, 2+, 0, 1−) Electron Transfer Series. *Inorg. Chem.* **2012**, *51*, 3707–3717.

(48) Van Stappen, C.; Maganas, D.; DeBeer, S.; Bill, E.; Neese, F. Investigations of the Magnetic and Spectroscopic Properties of V(III) and V(IV) Complexes. *Inorg. Chem.* **2018**, *57*, 6421–6438.

(49) Otto, S.; Nauth, A. M.; Ermilov, E.; Scholz, N.; Friedrich, A.; Resch-Genger, U.; Lochbrunner, S.; Opatz, T.; Heinze, K. Photo-Chromium: Sensitizer for Visible Light-Induced Oxidative C-H Bond Functionalization – Electron or Energy Transfer? *ChemPhotoChem* 2017, *1*, 344–349.

(50) Plasser, F.; Gómez, S.; Menger, M. F. S. J.; Mai, S.; González, L. Highly efficient surface hopping dynamics using a linear vibronic coupling model. *Phys. Chem. Chem. Phys.* 2019, *21*, 57–69.

TOC

555x458mm (150 x 150 DPI)

607x508mm (150 x 150 DPI)

1
2
3
4
5
6
7
8
9
10
11
12
13
14
15
16
17
18
19
20
21
22
23
24
25
26
27
28
29
30
31
32
33
34
35
36
37
38
39
40
41
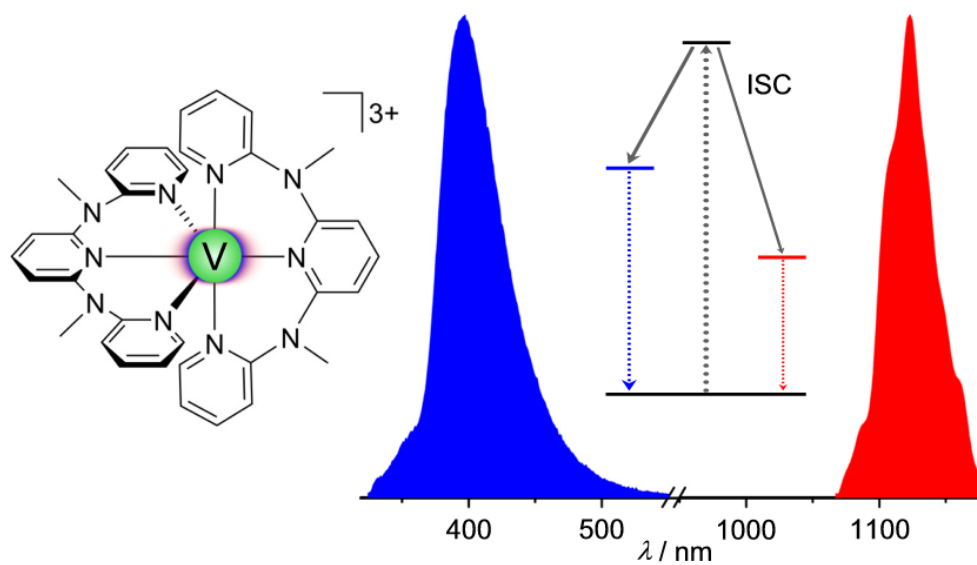42
43
44
45
46
47
48
49
50
51
52
53
54
55
56
57
58
59
60
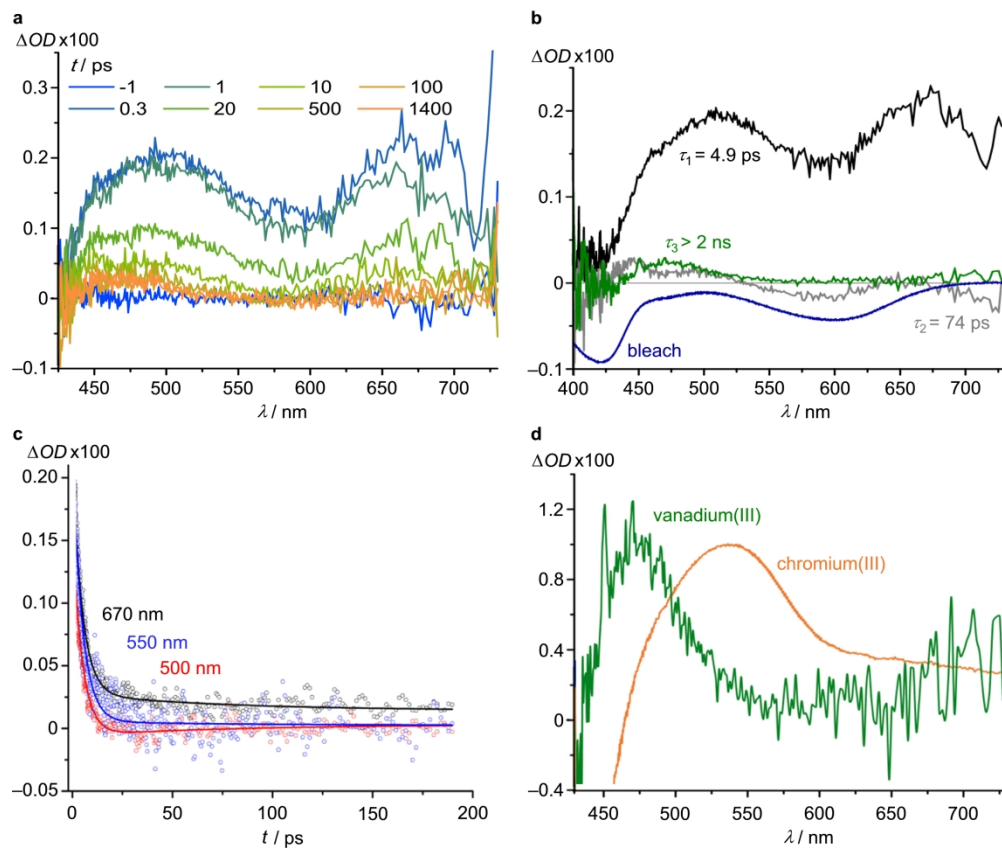
458x385mm (150 x 150 DPI)
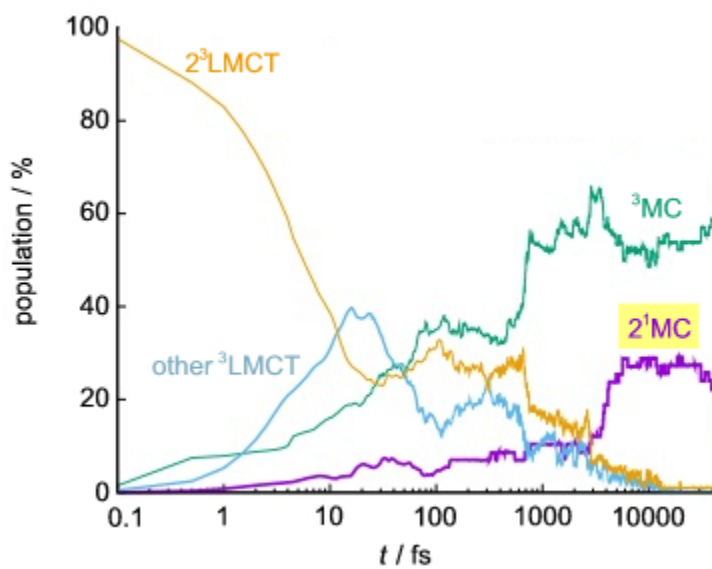
101x76mm (96 x 96 DPI)

71x40mm (300 x 300 DPI)